DAMAGE FUNCTIONS FOR THE VULNERABILITY ASSESSMENT OF MASONRY BUILDINGS SUBJECTED TO TUNNELLING

Giorgia Giardina[1], Max A.N. Hendriks[2], Jan G. Rots[3]

ABSTRACT

This paper describes a new framework for the assessment of potential damage caused by tunnelling induced settlement to surface masonry buildings. Finite elements models in two and three dimensions, validated through comparison with experimental results and field observations, are used to investigate the main factors governing the structural response to settlement. Parametric analyses are performed on the effect of geometrical and structural features, like the building dimensions, the nonlinear behaviour of masonry and the soil–structure interaction. The results are used to set a framework of an overall damage model, which correlates the analysed parameters with the risk for the building of being damaged by a certain settlement. The proposed vulnerability framework has the potential to be developed as a decision and management tool for the evaluation of the risk associated with underground excavations in urban areas.

Keywords: damage assessment, masonry buildings, settlement, tunnelling, vulnerability framework.

INTRODUCTION

In the area of tunnelling projects in urban areas, assessing the impact of the excavation on surface structures is an essential and complex component. The prediction of potential damage caused by tunnelling induced settlements is particularly challenging for masonry buildings, which represent the majority of historical structures. In addition to the uncertainties related to the soil movement prediction and the soil–structure interaction, also the unknowns in the masonry components and their mechanical proper-

[1]Research Associate, Department of Engineering, University of Cambridge, Trumpington Street, CB2 1PZ Cambridge, UK.

[2]Professor, Department of Structural Engineering, Norwegian University of Science and Technology, Rich. Birkelandsvei 1A, 7491 Trondheim, Norway and Department of Structural Engineering, Delft University of Technology, Stevinweg 1, 2628 CN Delft, The Netherlands.

[3]Professor, Department of Structural Engineering, Delft University of Technology, Stevinweg 1, 2628 CN Delft, The Netherlands.

ties need to be considered. Furthermore, both the soil and the masonry exhibit a nonlinear behaviour, which affects the global structural response.

Prospect of this research is the development of a new framework for the damage assessment, which relates the damage potentially caused to the building by the tunnelling induced ground deformations with the main parameters influencing the structural response to settlements, i.e. the building geometry, the amount of openings, the masonry and soil–structure interaction properties, the type of settlement profile. More specifically, a two-dimensional (2D) finite element model is used to investigate the effect of geometrical, material, loading and boundary conditions, while the effect of the tunnelling advance and the global torsional response of the structure are evaluated through sensitivity analyses performed on a three-dimensional (3D) model. To summarise the results of the numerical investigation two different damage models are proposed, based on polynomial and piecewise linear functions. Both models correlate the main building characteristics with the risk of being damaged by a certain level of settlement. The polynomial function gives the possibility to interpret the general sensitivity of each parameter to the expected damage. The piecewise linear functions allow to interpret the influence of each parameter on the expected moment of damage initiation and the subsequent progression of damage. The damage functions are based on the results of parametric analyses performed on 2D and 3D finite element models. The numerical models have been previously validated for a number of parameters through comparison with field data and experimental results.

In the following sections, after a brief overview of the state of the art, the description of the 2D and 3D finite element models used to investigate the structural response to settlements is given. Then, the results of the parametric study performed on the validated models are presented. Finally, the polynomial and piecewise linear damage functions are defined and evaluated on their capability to predict the numerical results and therefore to describe the global vulnerability of the structure.

LITERATURE REVIEW

The current assessment procedures apply the tunnelling induced greenfield displacements, calculated without considering the building influence, to a linear elastic beam representing the building. Geometrical properties corresponding to the ones of the building are assigned to the beam, together with equivalent shear and bending stiffness values; in this way, the strains induced by the soil displacements to the structure are evaluated. The comparison with limit values for the combination of shear, bending and tensile strains allows to classify the building according to the expected damage level (Burland and Wroth 1974; Boscardin and Cording 1989). Modified parameters based on numerical analyses, experimental tests and field data are included, to take into account the effect of the soil–structure interaction (Potts and Addenbrooke 1997; Franzius et al. 2006; Mair 2013).

Numerical studies performed on a 2D coupled model of building and soil revealed the limitations of the simplified linear-elastic model for the structure, which can lead to both too conservative or unconservative results (Netzel 2009). The damage prediction could therefore be improved by the use of computational approaches including plastic or cracking models for the masonry (Rots 2000; Son and Cording 2007; Giardina et al. 2013; Amorosi et al. 2014) and calibrated with experimental results (Laefer et al. 2011; Giardina et al. 2012). Furthermore, the combined effects of the main parameters governing the building vulnerability should be evaluated in a comprehensive damage model (Clarke and Laefer 2014).

NUMERICAL MODELS AND VALIDATION

The response of surface structures to tunnelling is a 3D problem: tunnel excavations cause a progressive 3D ground displacement field and the structural response depends on the 3D behaviour of the structure, e.g. in terms of torsion and effect of transverse walls. However, in the structural assessment, the ground deformations are generally decomposed in the transverse and longitudinal directions with respect to the tunnel axis. In this research, 2D and 3D models have been used to investigate different aspects of the problem. In particular, the 2D model has been used to derive information about the effect of openings, material properties, building weight, initial damage, normal and shear behaviour of the soil–structure interaction and type of settlement profile. The potential of the 3D model has been exploited to include the evaluation of aspect ratio of horizontal building dimensions, connection with adjacent structures, and position and alignment of the building with respect to the excavation.

This section describes the main features of the computational models adopted in this research and their validation through comparison with experimental and field data. An overview of the different characteristics of the models is given in Table 1.

2D finite element model

The 2D semi-coupled model reproduces the experimental test presented in Giardina et al. (2012). The test simulates the tunnelling-induced damage of a 1/10th scaled masonry façade. The structure is subjected to a controlled hogging deformation, which is considered the most dangerous for the surface building (Burland et al. 2001). The selected profile is comparable to the greenfield settlement induced by a 20 m deep tunnel driven in stiff clay, according to the analytical curve proposed by Peck (1969). The settlements are applied to a nonlinear interface accounting for the soil–structure interaction. This interface was characterised by no-tension, compression stiffness equivalent to a Dutch pile foundation (Rots 2000) and negligible stiffness in shear. The settlement profile is applied progressively in a number of steps, and therefore the results are also expressed relatively to the increasing applied deformation. The finite element model includes a smeared coaxial rotating crack model for the masonry, with linear tension softening after cracking. The interface between the façade and the steel beam was characterised by no-tension, assigned stiffness in compression and negligible stiffness in shear. The numerical model has been validated for the specific set of parameters adopted in the experimental test, showing the model capability to accurately reproduce the crack patterns and the deformation of the tested structure. More details can be found in Giardina et al. (2013).

3D finite element model

The limitations of the 2D modelling approach in simulating the progressive 3D displacement field induced by the excavation and the consequent torsional response of the building are overcome by the development of a 3D coupled model of building, foundation, soil and tunnel. Compared to the 3D models currently available in the literature (Augarde 1997; Liu 1997; Burd et al. 2000; Bloodworth 2002; Franzius 2003; Pickhaver et al. 2010), the main improvement of the presented approach consists in the introduction of a crack constitutive law with tension softening to simulate the progressive building damage on a masonry building. Coupling the different components allows reproducing the reciprocal influence between the building and the settlement profile. The tunnelling advance is simulated by a sequence of excavation steps: in each step a fixed value of ground volume loss is applied. As a consequence, all the analysis results refer to a fixed value of applied deformation, which corresponds to the imposed amount of volume loss. The 3D simulation of the structure and the tunnelling advance makes it possible to include the longitudinal settlement profile effect and the torsional building response. Since field measurements showed that the horizontal strain transmitted to the structure is often very small (Mair 2003), a smooth interface between the soil and the building is assumed. Following the same method applied to the 2D semi-coupled approach, the 3D modelling approach is validated through comparison with the monitoring data of a literature case study. Details about the model dimensions, loads, boundary conditions, material properties and the validation of the modelling approach are given in Boldrini (2011), Kappen (2012) and Giardina (2013).

PARAMETRIC STUDY

The numerical models have been used to perform a series of parametric analyses on the effect of geometrical aspects, material properties and boundary conditions on the building response to settlements.

Analysis variations

The sensitivity study analysed the following parameters:

- x_1 : percentage of façade openings (Fig. 1a)
- x_2 : fracture energy of masonry, G_f
- x_3 : Young's modulus of masonry, E
- x_4 : tensile strength of masonry, f_t
- x_5 : normal stiffness of the base interface, k_n
- x_{6s} : shear behaviour of the base interface
- x_{6t} : type of settlement profile (Fig. 1b)
- x_7 : orientation, O (Fig. 2)
- x_8 : grouping, G (Fig. 2)
- x_9 : position, P (Fig. 2)
- x_{10} : alignment, A (angle α in Fig. 2).

The values assumed in the parametric analyses performed on the 2D and 3D models are listed in Tables 2 and 3, respectively. For the amount of openings, masonry properties, interface parameters and settlement profile types, the variations were chosen to cover a wide range of scenarios. More details on the selection of each of these parameters can be found in Giardina (2013). The definitions of orientation, grouping and position were derived from the Building Risk Assessment (BRA) procedure (Guglielmetti et al. 2008). The orientation is defined as the aspect ratio between the building dimensions in the direction parallel (B) and perpendicular (L) to the tunnel axis. In the parametric study, three different conditions for the B/L ratio were analysed: $B/L < 0.5$ (O1), $0.5 < B/L < 2$ (O2) and $B/L > 2$ (O3). The grouping considers the modified lateral boundary conditions imposed by the presence of adjacent buildings: isolated building (no interior walls) with dimensions B and $L < 2D$ (G1), isolated building (no interior walls) with $B < 2L$ and $L > 2D$ (G2) and grouped building (two interior walls) perpendicular to the tunnel axis (G3), where D indicates the tunnel diameter. A full connection is assumed between the interior walls and the façades. The position is defined as the ratio between the horizontal tunnel-building distance d and the tunnel diameter D: $d/D < 1$ (P1), $1 < d/D < 3$ (P2) and $d/D > 3$ (P3). The alignment is the angle between the tunnel axis and the reference system of the building plant.

Damage indicators

The convenience of using numerical analyses in the framework of the existing damage classification system (Burland and Wroth 1974) strongly depends on the possibility of relating the finite element output to the required assessment input in terms of cracks. Therefore, for all the examined variations the structural damage is here evaluated in terms of maximum crack width. Other damage indicators, like horizontal strain and angular distortion, were also used to quantify the damage: the results of all evaluations are reported in Giardina (2013).

In the 2D analyses, the maximum crack width is derived from the relative displacements between two nodes on either side of the most pronounced crack. For the 3D models, the maximum crack width is calculated at the integration point level of the finite elements as $w_{\mathsf{max}} = \varepsilon_{cr,\mathsf{max}}\, h$, where $\varepsilon_{cr,\mathsf{max}}$ is the maximum crack strain and h is the pre-assumed crack bandwidth. The value of h is related to the average area A of the finite elements of the building, according to the formula $h = \sqrt{2A}$ (Slobbe et al. 2013), and it is equal to 566 mm. Compared to the methods used for the 2D models, this procedure allows for a more efficient data processing, which is especially relevant in case of 3D modelling. Local verifications have been performed to assure the comparability of the results.

As anticipated before, for the 3D analyses all the results refer to a fixed volume loss V_L of 2% (Fig. 3b), while for the 2D results the damage is expressed as a function of the applied deflection ratio $\hat{\Delta}$ (Fig. 3a). As a consequence, the 3D analyses offers additional information on the tunnelling advance and the 2D analyses offer additional information on the progression of the maximum crack width with the increasing applied deformation. For both the 2D and 3D results, the final damage in terms of maximum crack width is also translated into the corresponding damage class, according to Burland and Wroth

(1974) (Tab. 4). This allows for a direct comparison of the final assessment with the result of the application of the Limiting Tensile Strength Method (LTSM) to each single variation. The comparison is visualised as the ratio between the numerical and LTSM damage levels (damage level ratio).

Analysis results

To exemplify the procedure, the results corresponding to selected parameters for the sensitivity study performed on the 2D and 3D models are briefly illustrated. Starting with the 2D models, Figure 4 shows the maximum principal strain distribution and the deformed configuration at the maximum applied displacement of 11.5 mm (end of the experimental test) for the considered values of opening percentage (x_1). The small rectangular holes in all three models indicate additional vertical load applications, used in the scaled experiment to amplify the gravity: both in the experiment and in the model they work as imperfections in the façade. The contour plots indicate a strong localisation of the damage at the corner of the openings or at the imperfections, where the cracks defining the failure mechanism are concentrated. In the reference case, the first bending crack arises at the top of the façade, and progressively crosses the entire section in the vertical direction (Fig. 4c). Conversely, in the blind wall the increased stiffness reduces the initial bending, and the main crack develops horizontally, near the base (Fig. 4a). In the intermediate case, the failure mechanism presents both the horizontal and vertical cracks, but limited to the area around the largest window at the ground floor (Fig. 4b). Figure 4 also shows how the relatively high stiffness of the blind wall and the wall with the small openings leads to gapping in the no-tension interface, while in the reference case the façade follows more closely the applied settlement trough. According to Son and Cording (2007), the corresponding reduction in equivalent bending stiffness varies between 3 and 11$\%$ (for 10$\%$ of openings) and 20 and 26$\%$ (for 30$\%$ of openings), depending on the masonry properties.

The maximum crack width increases with the increase of openings. The damage level corresponding to the maximum crack width growth (Fig. 5a) confirms that for the analysed situation a façade with a larger amount of openings is more prone to the damage induced by the hogging settlement. The increased structural vulnerability due to the crack localisation and the reduced shear section has a much stronger effect than the increased bending flexibility given by more openings. As shown in Figure 5b, the LTSM only takes into account the latter effect, leading to a substantially higher damage level prediction for the two cases with openings, based on the numerical results compared to the LTSM prediction. More details about the physical interpretation of all the parametric results are given in Giardina (2013).

Following the same approach, the influence of the building orientation B/L on the structural damage is illustrated. By using the 3D model, the effect of building orientation was examined for different alignment, position and grouping conditions. For each of the combination sets shown in Table 3, only the orientation parameter was varied, while the other conditions were kept constant. Figure 6 illustrates the case of three grouped buildings (G3), adjacent (P1) and aligned (A0) to the tunnel axis.

For the orientation O1 and O2, the ratio B/L is modified by varying the dimension B of the transverse walls: the two buildings have the same dimension L in the direction perpendicular to the tunnel axis and they are subjected to both sagging and hogging type of settlements. Consistently with field observations (Burland et al. 2001), the structure is more vulnerable to the hogging deformation, and therefore the failure mechanism corresponds to the typical hogging-induced damage, with two main vertical cracks starting form the façade top. The response is magnified by the modelling assumption of neglecting the influence of the roof. For the O3 case the increased B/L ratio is obtained by reducing the L dimension, and therefore the building falls entirely into the sagging area of the settlement profile. As a consequence, its failure mechanism is characterised by a vertical crack at the façade base, worsened by the rotation of the load bearing transverse walls, during the excavation phases under the building (Stage 9 in Fig. 6). Figure 6 includes the visualisation of the base interface normal stresses. The vector plots reveal that the building weight and live loads keep the interface compressed; local unloading is visible below the main cracks.

In Figure 7 the damage levels for this variation are compared with the ones resulting from the other analysed combinations, i.e. single buildings (G1) located at different positions with respect to the tunnel axis (P1, P2, P3). The graphs show that for the selected case (G3-P1-A0) the global damage is moderate for all the assumed values of B/L. In case of a single building (G1), for equal dimension L, the damage tends to increase when increasing the longitudinal dimension B (orientation O1 and O2 of the curves G1-P2-A0 and G1-P3-A0). This happens because the connection between the two façades offered by the transverse walls becomes more flexible, and therefore the stiffening effects against the deformation induced by the transverse settlement profile is reduced. When the B/L ratio increases by decreasing L, the tilting component of the building distortion becomes dominant and the risk of damage is reduced. This is consistent with the vulnerability coefficients derived by Guglielmetti et al. (2008), which indicate an increased vulnerability with the increase of the façade dimension in the direction transverse to the tunnel axis. A similar effect occurs when a series of adjacent buildings are connected via common transverse walls. Grouped buildings suffer from more severe damage than short isolated buildings, which tend to tilt more rigidly. The position parameter affects simultaneously the magnitude and the type of settlement. The damage generally decreases with the increase of distance from the tunnel, due to the reduction of settlement values (Guglielmetti et al. 2008). Buildings located in the proximity of the tunnel (sagging zone) and characterised by a compact geometry and thus by a stiffer global response represent an exception to this trend. A detailed interpretation of the effect of grouping, position and alignment parameters on the structural response is presented in Giardina (2013).

Figures 8 and 9 report the results in terms of damage level for all the analyses performed on the 2D and 3D model, respectively. The results underline the high dependency of the final damage on the material cracking and the soil–structure interaction, which should therefore be included in the structural response evaluation. In particular, the quantified influence of the interface normal stiffness support the studies oriented to the evaluation of the relative stiffness between the building and the soil (Potts and Addenbrooke 1997; Franzius 2003; Goh and Mair 2011). The effect of masonry fracture energy and tensile strength emphasises the importance of an appropriate level of knowledge of the material properties, which could be obtained through preliminary non-destructive tests.

VULNERABILITY FRAMEWORK

The quantitative results of the variational study are used to set the framework of an alternative damage classification system.

The selected damage function d depends on a certain number of parameters x_i, collected in an array $\mathbf{x}$: $d = d(\hat{\Delta}, \mathbf{x})$. The damage function approximates the data points d_{num} resulting from the parametric analyses performed on the 2D and 3D models. In the 2D case the dependency on the deflection ratio $\hat{\Delta}$ is also explicitly considered. The approximated solution of the system $d(\hat{\Delta}, \mathbf{x}) \cong d_{\mathrm{num}}(\hat{\Delta}, \mathbf{x})$ is obtained by minimising the sum of squares $\sum_{f=1}^{k} \sum_{s=1}^{l} (d^f(\hat{\Delta}_s,\ \mathbf{x}) - d^f_{\mathrm{num}}(\hat{\Delta}_s,\ \mathbf{x}))^{\mathbf{2}}$, where $k = 14+$

$15 = 29$ is the total amount of 2D and 3D variation studies, the superscript f indicates the individual numerical analyses, $l = 24$ is the total amount of deflection ratios considered, between 0 and 3×10^{-3}, and s indicates each individual deflection ratio.

Damage functions

Two alternative damage functions are used to fit the numerical results: a polynomial and a piecewise linear function. The polynomial functions approximating the 2D and 3D results are defined as:

$$d'_{\text{2D}}(\hat{\Delta}, \overline{\mathbf{x}}) = d_{\text{2D,ref}}(\hat{\Delta}) + \sum\nolimits_{i=1}^{6} a_i \overline{x}_i = b_1 + b_2\hat{\Delta} + b_3\hat{\Delta}^2 + b_4\hat{\Delta}^3 + \sum\nolimits_{i=1}^{6} a_i \overline{x}_i \tag{1}$$

$$d'_{\text{3D}}\left(\overline{\mathbf{x}}\right) = d_{\text{3D,ref}} + \sum\nolimits_{i=7}^{10} a_i \overline{x}_i = b_5 + \sum\nolimits_{i=7}^{10} a_i \overline{x}_i \tag{2}$$

where $d_{\text{2D,ref}}$ and $d_{\text{3D,ref}}$ are the selected reference values for the 2D and 3D variations, respectively, a_i and b_i are the polynomial coefficients and $\overline{\mathbf{x}}$ contains normalised values of the parameters x_i. The normalised parameters $\overline{x_i}$ will be described in the next subsection. Note that both functions are linear in the parameter $\overline{x_i}$.

The 2D analyses have been carried out by imposing a certain deformation to the interface at the façade base, and therefore the 2D damage function depends on both the deflection ratio $\hat{\Delta}$ and the analysed parameters $\overline{x_i}$. A third order polynomial is chosen to fit the numerical results. A preliminary fitting of the reference case, which corresponds to the experimentally tested façade, showed that a cubic polynomial is the lowest degree that guarantees a good approximation of the numerical curve (Fig. 10a). Conversely, the 3D analyses simulated the tunnel advance for a fixed value of volume loss $V_L = 2\%$, and therefore the 3D damage function does not depend on the applied deformation.

Defining the damage function as the sum of the normalised parameters multiplied by coefficients a_i gives a relatively simple expression, which has the main advantage of making the relative weight of each parameter explicit. However, the 2D numerical analysis curves are typically characterised by a steady increase of damage after a longer or shorter latency and before reaching a certain damage level plateau; a piecewise linear function with three intervals for ranges of $\hat{\Delta}$ depending on the parameters $\overline{x_i}$ was therefore adopted as alternative damage function (Fig. 10b). This second model for the 2D results can be written as:

$$d''_{\mathrm{2D}}\left(\hat{\Delta},\overline{\mathbf{x}}\right)=\begin{cases}1 & \text{for}\quad \hat{\Delta}\le\hat{\Delta}_1\\ 1+5\,\dfrac{\hat{\Delta}-\hat{\Delta}_1}{\hat{\Delta}_2-\hat{\Delta}} & \text{for}\quad \hat{\Delta}_1\le\hat{\Delta}\le\hat{\Delta}_2\\ 6 & \text{for}\quad \hat{\Delta}\ge\hat{\Delta}_2\end{cases}\tag{3}$$

where

$$\hat{\Delta}_1=c_0+\sum\nolimits_{i=1}^{6}c_i\overline{x}_i\tag{4}$$

$$\hat{\Delta}_2=d_0+\sum\nolimits_{i=1}^{6}d_i\overline{x}_i\tag{5}$$

are the deflection ratio values corresponding to the onset of damage and to the maximum damage, respectively (Fig. 10b). From the difference $\hat{\Delta}_2-\hat{\Delta}_1=d_0-c_0+\sum_{i=1}^{6}(d_i-c_i)\overline{x}_i$ it follows that (d_i-c_i) is a measure of the damage progression rate (Fig. 10b).

Normalised parameters

Normalising the range of each parameter $\overline{x}_i$ to a unit range facilitates the interpretation of the coefficients a_i, c_i and d_i. The normalised parameters are defined as:

$$\overline{x}_1=\frac{x_1-x_{1\mathrm{ref}}}{30}\qquad \overline{x}_1\in[-1,\ 0]\tag{6}$$

$$\overline{x}_2=\frac{x_2-x_{2\mathrm{ref}}}{990}\qquad \overline{x}_2\in[0,\ 1]\tag{7}$$

$$\overline{x}_3=\frac{x_3-x_{3\mathrm{ref}}}{8000}\qquad \overline{x}_3\in\left[-{}^1\!/_4,\ {}^3\!/_4\right]\tag{8}$$

$$\overline{x}_4=\frac{x_4-x_{4\mathrm{ref}}}{0.8}\qquad \overline{x}_4\in[0,\ 1]\tag{9}$$

$$\overline{x}_5=\frac{\log_{10}x_5-\log_{10}x_{5\mathrm{ref}}}{2}\qquad \overline{x}_5\in[-1,\ 0]\tag{10}$$

$$\overline{x}_6=\begin{cases}0 & \text{if}\quad (x_{6s},x_{6t})=(\text{smooth},\text{hogging})\quad\text{or}\quad(\text{rough},\text{sagging})\\ 1 & \text{if}\quad (x_{6s},x_{6t})=(\text{smooth},\text{sagging})\quad\text{or}\quad(\text{rough},\text{hogging})\end{cases}\tag{11}$$

$$\overline{x}_7=\begin{cases}-{}^1\!/_2 & \text{if}\quad x_7=\mathrm{O1}\\ 0 & \text{if}\quad x_7=\mathrm{O2}\\ {}^1\!/_2 & \text{if}\quad x_7=\mathrm{O3}\end{cases}\tag{12}$$

$$\overline{x}_8=\begin{cases}0 & \text{if}\quad x_8=\mathrm{G1}\\ {}^1\!/_2 & \text{if}\quad x_8=\mathrm{G2}\\ 1 & \text{if}\quad x_8=\mathrm{G3}\end{cases}\tag{13}$$

$$\overline{x}_9=\begin{cases}-{}^1\!/_2 & \text{if}\quad x_9=\mathrm{P1}\\ 0 & \text{if}\quad x_9=\mathrm{P2}\\ {}^1\!/_2 & \text{if}\quad x_9=\mathrm{P3}\end{cases}\tag{14}$$

$$\overline{x}_{10}=\frac{||x_{10}|-90|-90}{90}\qquad \overline{x}_{10}\in[-1,\ 0]\tag{15}$$

where $x_{i\mathrm{ref}}$ are the parameter values in the reference case.

The normalised parameters $\overline{x}_i$ are formulated such as to become zero at the reference case: for each parameter the normalisation to a unit range is based on the domain of values assumed in the sensitivity study. For example, in the analysis of the opening amount influence, the considered values are 0, 10 and 30$\%$ of openings, being 30$\%$ the reference value, and therefore the difference between x_1 and x_{1ref} in Equation 6 is divided by 30.

The normalised parameters from $\overline{x}_1$ to $\overline{x}_4$ are linearly related to the respective parameters x_i. The interface normal stiffness x_5 can vary over several orders of magnitude; $\overline{x}_5$ indicates the order of magnitude by using a logarithmic function. The effect of the base interface shear behaviour depends on the applied profile of horizontal deformations, which is determined by the position of the structure with respect to the tunnel (e.g. sagging or hogging area). For this reason, the influence of parameters x_{6s} and x_{6t} is coupled in the $\overline{x}_6$ formulation. According to Equation 11, an increase of damage is expected for the combination of a smooth interface in the sagging zone and a rough interface in the hogging zone. This formulation interprets a general trend observed by previous research (Netzel 2009; Giardina 2013). The highest value of $\overline{x}_6$ is executed to lead to an increase of damage with respect to the reference case. The definition of $\overline{x}_{10}$ takes into account the observation that in the hogging area the building is more vulnerable when its façades are aligned with the transverse settlement profile, thus $x_{10} = 0°, 180°$ (Giardina 2013). Although such a trend cannot be deduced for the sagging area, the $\overline{x}_{10}$ formulation does not take the interaction between alignment and type of settlement profile into account. An increase in $\overline{x}_{10}$ is expected to lead to an increase of damage.

The final damage level resulting from the numerical simulations, which was related to the maximum crack width by means of a step function ranging from 1 to 6 (Tab. 4), is now smoothened into a continuous function of the maximum crack width, as illustrated in Figure 11.

RESULTS

In this section, first the performance of the two damage models based on the polynomial and the piecewise linear functions in predicting the 2D numerical results are compared; then the results of the polynomial function based damage model when applied to the sensitivity analysis performed on the 3D model are presented. Figure 12 shows the comparison between the data from the 2D analysis and the fitted damage functions. The damage functions are obtained by fitting the results of all the progressive

24 values of Δ/L applied in the 14 numerical analyses, leading to the evaluation of 336 observations. Considering the relative simplicity of both damage functions with a limited number of coefficients compared to the number of observations and the number of influence parameters, the damage models show an adequate flexibility in predicting the damage level as a function of the applied deformations. Approximations offered by the polynomial function appear to deviate when the shape of the numerical curve is particularly steep, i.e. the damage rapidly increases for a small increment of applied deformation, due to the brittle behaviour of masonry. This deviation between the numerical analysis and the estimated curves is probably mainly due to the selected shape of the first part of the damage function, which is a third degree polynomial function with constant coefficients b_i. The values of the coefficients a_i, b_i, c_i and d_i are reported in Table 5.

Compared to the polynomial, the piecewise linear function can better capture the sudden change of slope corresponding to the cracking initiation, and in general gives a better approximation of the numerical data afterwards. The solution offered by the piecewise linear function is also generally more conservative, in relation to the numerical results. Exceptions are represented by the cases where the intermediate parameter value does not lead to an intermediate damage behaviour, with respect to the two extreme parameter values. For example, an increase of tensile strength from $f_t = 0.1$ MPa to $f_t = 0.9$ MPa leads to a global reduction of vulnerability (Fig. 12d). However, the intermediate case $f_t = 0.3$ MPa presents a local sudden increase of slope around $\hat{\Delta} = 1 \times 10^{-3}$, which is underestimated by the damage curve. Another example of this behaviour can be detected in the interface normal stiffness variations (Fig. 13a). Since a stiffer interface is leading to a general higher level of damage, the damage functions for the intermediate case tend to predict an intermediate level of damage, underestimating the local brittle behaviour shown in Figure 13a2.

On average, the damage functions can give a reasonable approximation of all the selected curves. Exceptions are represented by the combinations between the type of settlement profile and the shear behaviour of the interface (Figs. 13b2, 13c1 and 13c2). The reason can be the local discrepancy between the assumed formulation of $\overline{x}_6$ (Eq. 11) and the observed interaction of factors x_{6s} and x_{6t} representing the shear behaviour of the base interface and the type of applied settlement, respectively.

Figure 14 shows the comparison between the averaged 3D results and the prediction offered by the polynomial damage function. More than one analysis set were available for the orientation, position and alignment variation; in order to reduce the influence of the relatively arbitrary selection of cases included in the sensitivity study, the results were preliminary averaged for these variations, resulting in a similar weight for the four variations. The average values, which are used as data in the least square procedure, are connected by grey lines. As for the 2D study, the model is able to interpret the trends of the parameter variations. The accuracy of the prediction is limited by the choice of adopting a damage function, which is linear in the parameters $\overline{x}$. However, the choice of a multilinear damage function (Eq. 2) facilitates the interpretation of the obtained coefficients a_i, as the value of a_i indicates possible increases of damage levels by varying the corresponding parameter x_i.

Figure 15a visualises the values of the coefficients a_i of the polynomial functions. The absolute value of each coefficient indicates its relative influence on the structural damage level, while the sign of each coefficient indicates the relation between a variation of the corresponding parameter value and the increase or decrease of building vulnerability. Figure 15b illustrates the additional interpretation of the parametric results offered by the piecewise linear function. Whereas the parameter a_1 would be interpreted as increase or decrease of damage level, the parameters c_i and d_i would be interpreted as increase or decrease of the critical deflection ratios $\hat{\Delta}_1$ and $\hat{\Delta}_2$ (Eq. 4 and 5). Parameters c_i represent the effect of each parameter on the crack initiation, while the difference between d_i and c_i is a measure of the crack propagation rate. The structural behaviour becomes more brittle for an increasing value of parameter $\overline{x}_i$ when $d_i - c_i < 0$, while the cracking propagates at lower rate, i.e. more ductile, for increasing $\overline{x}_i$ if $d_i - c_i > 0$.

For example the value of the coefficient a_1 related to the opening percentage parameter x_1 (Fig. 15a) shows that an increase of openings from 0 to 30$\%$ of the façade surface increases the structural vulnerability up to 2 damage levels. The positive sign of the coefficient indicates a positive correlation between the value of the parameter and the damage level variation (see Fig. 5a). The corresponding coefficients c_1 and d_1 (Fig. 15b) indicate that the opening percentage has a limited influence on the onset of damage, while it has a relatively larger influence on the rate of damage afterwards. Since

$d_i - c_i < 0$, the structure becomes more brittle for smaller values of opening percentage, due to a higher initial stiffness.

For the fracture energy parameter x_2, Figure 15a indicates that the analysed variations can lead to an increased damage of up to 3 levels, with the structure becoming less vulnerable as the fracture energy of the masonry increases (negative coefficient, see Fig. 8a). Figure 15b shows that in this case the governing effect of the influence on the damage progression rate is even more visible than for the amount of openings. Furthermore, the positive value of $d_i - c_i$ indicates that the structure becomes more ductile for higher values of fracture energy, i.e. the deflection ratio at which the maximum damage is reached becomes larger.

From Figure 15a it can be seen that the interface normal stiffness representing the soil–structure interaction and the nonlinear behaviour of the masonry are the most important parameters governing the settlement-induced structural damage. For the adopted parameter variations, they can vary the final risk assessment by up to four damage levels. These values give an estimation of the impact of neglecting these two fundamental aspects of the structural response in the damage assessment. They also quantify reductions of limiting tensile strain values that could be implemented in the current empirical analytical procedure (LTSM) in order to include these effects. The relatively little effect of the Young's modulus variation can be explained by the assumption of a smeared crack model with tension-softening behaviour for the masonry. The influence of a lower Young's modulus is in fact negligible, if compared with the global stiffness reduction induced by the cracking.

Among the characteristics evaluated through the 3D analysis, Figure 15a indicates the governing role of the connection with adjacent structures, which affects the lateral boundary conditions and the global stiffness of the building in relation to the applied settlement profile. The grouping parameter could induce a variation up to three levels in the final damage assessment.

The damage function evaluates the alignment of the building with respect to the tunnel axis as the second most important parameter of the 3D study, while the aspect ratio between the horizontal building dimensions has a very marginal role. However, the orientation and alignment parameters, referring both to the direction of the most vulnerable structural elements with respect to the governing settlement profile, are closely interacting. Given the proposed modelling approach and vulnerability framework, the numerical analyses could be extended to a more exhaustive investigation of the relation between the two parameters, for example performing the alignment variation for different types of orientation.

CONCLUSION

This paper proposes a global formulation of the vulnerability of masonry buildings subjected to tunnelling-induced settlements, based on parametric numerical analyses. The construction and verification of the proposed vulnerability framework is based on the following methodological steps:

1. Development and validation of 2D and 3D numerical models able to capture the response of masonry buildings to tunnelling;
2. Sensitivity study, performed on the numerical models, to investigate the effect of the main factors governing the structural response and damage;
3. Use of the parametric results to build a damage model based on polynomial and piecewise linear functions, which correlate the analysed factors with the building vulnerability;
4. Verification of the damage model ability to predict the available numerical results.

The main findings of the paper can be summarised as follows:

- The polynomial function sets a linear dependency between the final response and the selected parameters, with coefficients representing the relative weight of each parameter. The piecewise function gives a further opportunity to interpret the effect of each parameter variation on the initiation and progression of damage.
- The adopted normalisation of parameters has the main advantage of making possible a direct comparison between the selected parameter values and the consequent increase or decrease of the potential structural damage level (polynomial function) and the consequent increase or decrease of critical deflection ratios (piecewise linear function). This improves the accessibility of the obtained results.
- By incorporating the results of the 2D and 3D parametric analyses, the damage model provides an overall evaluation of the principal factors governing the building response. The damage model outcomes have shown the major influence of the masonry cracking model, the soil–structure interface normal stiffness and the lateral building constraints.

- The proposed damage function makes possible a quantitative assessment of the damage risk variation as defined by the empirical analytical procedure currently used in practice. For example, in case of a masonry façade preliminary classified as subjected to moderate risk of damage, the presence of a large amount of windows can increase the damage category up to two levels, indicating the need for settlement mitigating measurements or building strengthening techniques.
- The results in terms of parameter weights on the structural response can be used to refine the total strain limit values included in the LTSM, according to the building characteristics. The proposed model has therefore the potential to be developed as a decision and management tool for the assessment of the settlement-induced damage to buildings.
- Due to its flexible formulation, the method might serve as a growing knowledge system, which would be improved by the inclusion of new input data, e.g. field measurements from actual projects and additional experimental and numerical results.

REFERENCES

Amorosi, A., Boldini, D., De Felice, G., Malena, M., and Sebastianelli, M. (2014). "Tunnelling-induced deformation and damage on historical masonry structures." *Géotechnique*, 64, 118–130(12).

Augarde, C. E. (1997). "Numerical modelling of tunnelling processes for assessment of damage to buildings." Ph.D. thesis, University of Oxford, Oxford.

Bloodworth, A. G. (2002). "Three-dimensional analysis of tunnelling effects on structures to develop design methods." Ph.D. thesis, University of Oxford, Oxford.

Boldrini, S. (2011). "Damage assessment of buildings including explicit soil-structure interaction." M.S. thesis, Sapienza University, Rome.

Boscardin, M. D. and Cording, E. J. (1989). "Building response to excavation-induced settlement." *Journal of Geotechnical Engineering*, 115(1), 1–21.

Burd, H. J., Houlsby, G. T., Augarde, C. E., and Liu, G. (2000). "Modelling tunnel-induced settlement of masonry buildings." *ICE Proceedings: Geotechnical Engineering*, Vol. 143, 17–29.

Burland, J, B., Standing J, R., and Jardine F, M. (2001). *Building response to tunnelling: case studies from construction of the Jubilee Line Extension, London*. CIRIA Special Publication Series. Thomas Telford, London.

Burland, J. P. and Wroth, C. P. (1974). "Settlement of buildings and associated damage." *Proceedings of Conference on Settlement of Structures*, Cambridge, Pentech Press, 611–654.

Clarke, J. A. and Laefer, D. F. (2014). “Evaluation of risk assessment procedures for buildings adjacent to tunnelling works.” *Tunnelling and Underground Space Technology*, 40(0), 333 – 342.

Franzius, J. N. (2003). “Behaviour of buildings due to tunnel induced subsidence.” Ph.D. thesis, Imperial College, London.

Franzius, J. N., Potts, D. M., and Burland, J. B. (2006). “Twist behaviour of buildings due to tunnel induced ground movement.” *Proceedings of the 5th International Conference on Geotechnical Aspects of Underground Construction in Soft Ground*, E. Kwast, K. Bakker, W. Broere, and A. Bezuijen, eds., Amsterdam, Taylor and Francis, 107–113.

Giardina, G. (2013). “Modelling of settlement induced building damage.” Ph.D. thesis, Delft University of Technology, Delft.

Giardina, G., Marini, A., Hendriks, M. A. N., Rots, J. G., Rizzardini, F., and Giuriani, E. (2012). “Experimental analysis of a masonry façade subject to tunnelling-induced settlement.” *Engineering Structures*, 45, 421–434.

Giardina, G., van de Graaf, A., Hendriks, M. A. N., Rots, J. G., and Marini, A. (2013). “Numerical analysis of a masonry façade subject to tunnelling-induced settlement.” *Engineering Structures*, 54, 234–247.

Goh, K. H. and Mair, R. J. (2011). “The response of buildings to movements induced by deep excavations.” *Geotechnical Engineering Journal of the SEAGS and AGSSEA*, 42(3).

Guglielmetti, V., Grasso, P., Mahtab, A., and Xu, S. (2008). *Mechanized tunnelling in urban areas: design methodology and construction control*. Taylor and Francis.

Kappen, J. M. J. (2012). “Three-dimensional numerical analysis of tunnelling induced damage: the influence of masonry building geometry and location.” M.S. thesis, Delft University of Technology, Delft.

Laefer, D. F., Hong, L. T., Erkal, A., Long, J. H., and Cording, E. J. (2011). “Manufacturing, assembly, and testing of scaled, historic masonry for one-gravity, pseudo-static, soil-structure experiments.” *Construction and Building Materials*, 25(12), 4362–4373.

Liu, G. (1997). “Numerical modelling of settlement damage to masonry structures caused by tunnelling.” Ph.D. thesis, University of Oxford, Oxford.

Mair, R. J. (2003). “Research on tunnelling-induced ground movements and their effects on buildings-lessons from the jubilee line extension. keynote lecture.” *Proceedings of the International Conference on Response of Buildings to Excavation-Induced Ground Movements*, M. Jardine, F, ed., 199, CIRIA Special Publication, 3–26.

Mair, R. J. (2013). “Tunnelling and deep excavations: ground movements and their effects.” *Proceedings of the 15th European Conference on Soil Mechanics and Geotechnical Engineering - Geotechnics of Hard Soils - Weak Rocks (Part 4)*, A. e. a. Anagnostopoulos, ed., IOS Press, 39–70.

Netzel, H. D. (2009). “Building response due to ground movements.” Ph.D. thesis, Delft University of Technology, Delft.

Peck, R. B. (1969). “Deep excavations and tunneling in soft ground.” *Proceedings of the 7th International Conference on Soil Mechanics and Foundation Engineering*, Mexico City, 225–290.

Pickhaver, J. A., Burd, H. J., and Houlsby, G. T. (2010). “An equivalent beam method to model masonry buildings in 3D finite element analysis.” *Computers and Structures*, 88(19-20), 1049–1063.

Potts, D. M. and Addenbrooke, T. I. (1997). “A structure’s influence on tunnelling-induced ground movements.” *Proceedings of the Institution of Civil Engineers: Geotechnical Engineering*, 125(2), 109–125.

Rots, J. G. (2000). “Settlement damage predictions for masonry.” *Maintenance and restrengthening of materials and structures – Brick and brickwork. Proceedings of the International Workshop on Urban Heritage and Building Maintenance*, L. Verhoef and F. Wittman, eds., Freiburg, Aedificatio, 47–62.

Slobbe, A. T., Hendriks, M. A. N., and Rots, J. G. (2013). “Systematic assessment of directional mesh bias with periodic boundary conditions: Applied to the crack band model.” *Engineering Fracture Mechanics*, 109, 186–208.

Son, M. and Cording, E. J. (2007). “Evaluation of building stiffness for building response analysis to excavation-induced ground movements.” *Journal of Geotechnical and Geoenvironmental Engineering*, 133(8), 995–1002.

List of Tables

TABLE 1: Main features of the 2D and 3D finite element models used to perform the parametric study.

Model	**2D semi-coupled**	**3D coupled**
Scale	Scaled	True scale
Structure	Masonry façade of a typical historic Dutch house	Masonry building reproducing a typical historic Dutch house
Settlement	Fixed transversal settlement of increasing amplitude	Propagating 3D settlement of fixed amplitude
Variations	Openings, material properties, building weight, initial damage, normal and shear behaviour of the soil–structure interface, type of settlement profile	Aspect ratio of horizontal building dimensions, connection with adjacent structures, position and alignment of the building with respect to the excavation

TABLE 2: Parameter variations of the 2D sensitivity study. The term ”rough” indicate a base interface with a tangential stiffness of $0.7 \times 10^9 \mathrm{N/m}^3$. See Giardina (2013) for further details.

	Openings	G_f	E	f_t	k_n	Interf. shear behaviour	Trough
f	x_1	x_2	x_3	x_4	x_5	x_{6s}	x_{6t}
	(%)	(N/m)	(MPa)	(MPa)	$(\mathrm{N/m}^3)$	(–)	(–)
ref	30	10	3000	0.1	0.7×10^9	smooth	hogging
1	0	10	3000	0.1	0.7×10^9	smooth	hogging
2	10	10	3000	0.1	0.7×10^9	smooth	hogging
3	30	50	3000	0.1	0.7×10^9	smooth	hogging
4	30	1000	3000	0.1	0.7×10^9	smooth	hogging
5	30	10	1000	0.1	0.7×10^9	smooth	hogging
6	30	10	9000	0.1	0.7×10^9	smooth	hogging
7	30	10	3000	0.3	0.7×10^9	smooth	hogging
8	30	10	3000	0.9	0.7×10^9	smooth	hogging
9	30	10	3000	0.1	0.7×10^7	smooth	hogging
10	30	10	3000	0.1	0.7×10^8	smooth	hogging
11	30	10	3000	0.1	0.7×10^9	rough	hogging
12	30	10	3000	0.1	0.7×10^9	smooth	sagging
13	30	10	3000	0.1	0.7×10^9	rough	sagging

TABLE 3: Parameter variations of the 3D sensitivity study.

f	x_7 (–)	x_8 (–)	x_9 (–)	x_{10} (°)
ref	O2	G1	P2	0
1	O1	G1	P2	0
2	O3	G1	P2	0
3	O2	G2	P2	0
4	O2	G3	P2	0
5	O2	G1	P1	0
6	O2	G1	P3	0
7	O2	G1	P2	22.50
8	O2	G1	P2	45.00
9	O2	G1	P2	67.50
10	O2	G1	P2	90.00
11	O2	G1	P2	112.50
12	O2	G1	P2	135.00
13	O2	G1	P2	157.00
14	O2	G1	P2	180.00

TABLE 4: Damage classification of masonry buildings as a function of the maximum crack width.

Damage level	**Damage class**	**Crack width**
1	Negligible	up to 0.1 mm
2	Very slight	up to 1 mm
3	Slight	up to 5 mm
4	Moderate	5 to 15 mm
5	Severe	15 to 25 mm
6	Very severe	>25 mm

TABLE 5: Coefficients of the damage functions.

Coefficient	Value	Coefficient	Value
a_1	2.23	c_0	2.21×10^{-4}
a_2	-3.16	c_1	-8.58×10^{-4}
a_3	6.48×10^-2	c_2	-6.38×10^{-4}
a_4	-3.04	c_3	-1.09×10^{-4}
a_5	3.68	c_4	-4.75×10^{-4}
a_6	1.04	c_5	-8.41×10^{-4}
a_7	-8.00×10^-2	c_6	-2.31×10^{-4}
a_8	2.91	d_0	6.35×10^{4}
a_9	6.42×10^-1	d_1	-2.80×10^{3}
a_{10}	1.02	d_2	1.48×10^{2}
b_1	1.91	d_3	4.75×10^{4}
b_2	3.72×10^{3}	d_4	1.40×10^{2}
b_3	-1.29×10^{6}	d_5	-1.30×10^{2}
b_4	1.72×10^{8}	d_6	2.78×10^{4}
b_5	1.75		

List of Figures

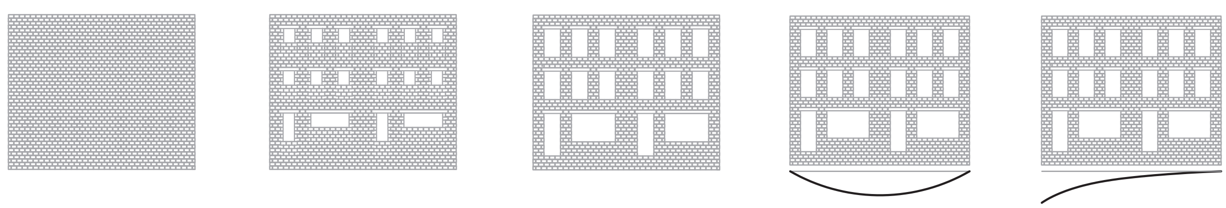

(a) 0%, 10% and 30% (reference case) of openings.

(b) sagging and hogging (reference case) settlement profile.

FIG. 1: Variations of (a) amount of openings and (b) settlement profile.

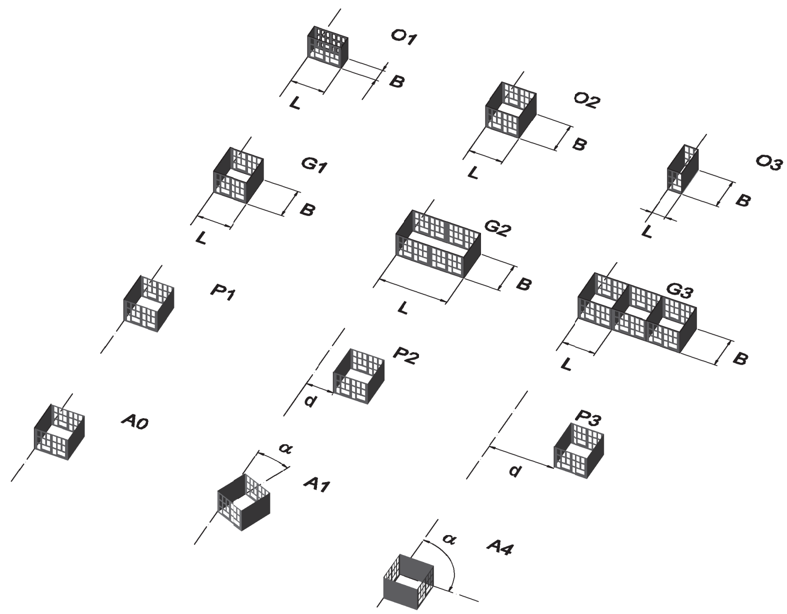

FIG. 2: Overview of the parameters that were varied in the 3D sensitivity study: orientation O, grouping G, position P and alignment A.

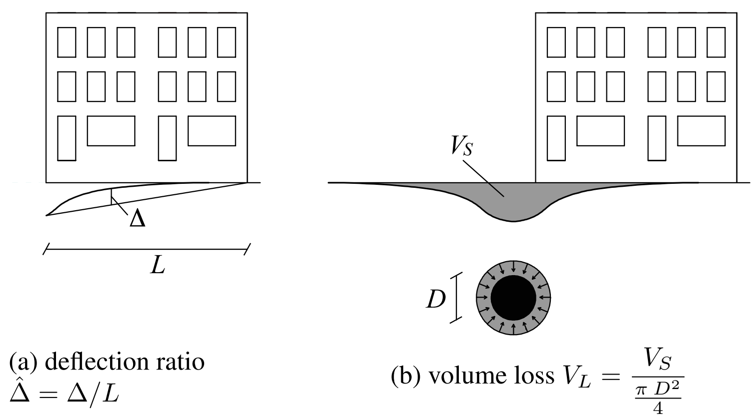

FIG. 3: Indicators of the applied deformation for the (a) 2D and (b) 3D analyses.

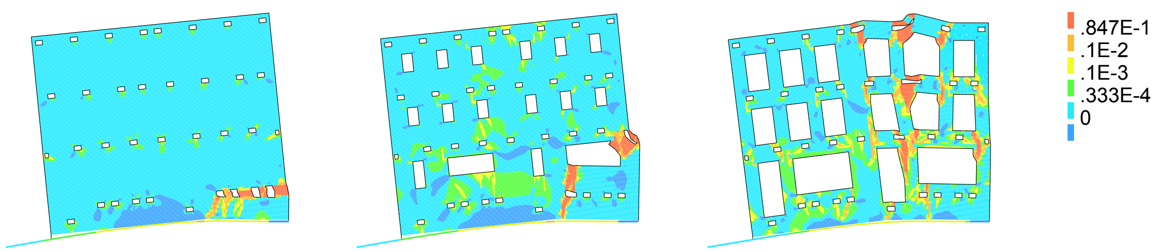

(a) 0%

(b) 10%

(c) 30%

FIG. 4: Maximum principal strain distribution and deformed configuration at 11.5 mm of applied displacement, for different values of opening percentage x_1: analyses 1, 2 and reference case (see Tab. 2).

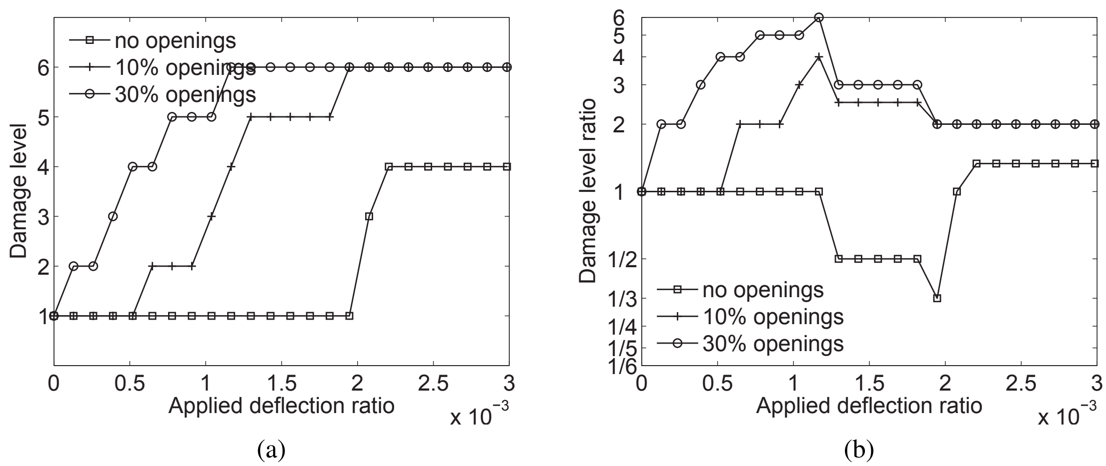

FIG. 5: Variation of opening percentage: numerical damage level (a) and ratio between numerical and LTSM damage levels (in logarithmic scale) (b) as a function of the applied deflection ratio, according to analyses 1, 2 and reference case (see Tab. 2).

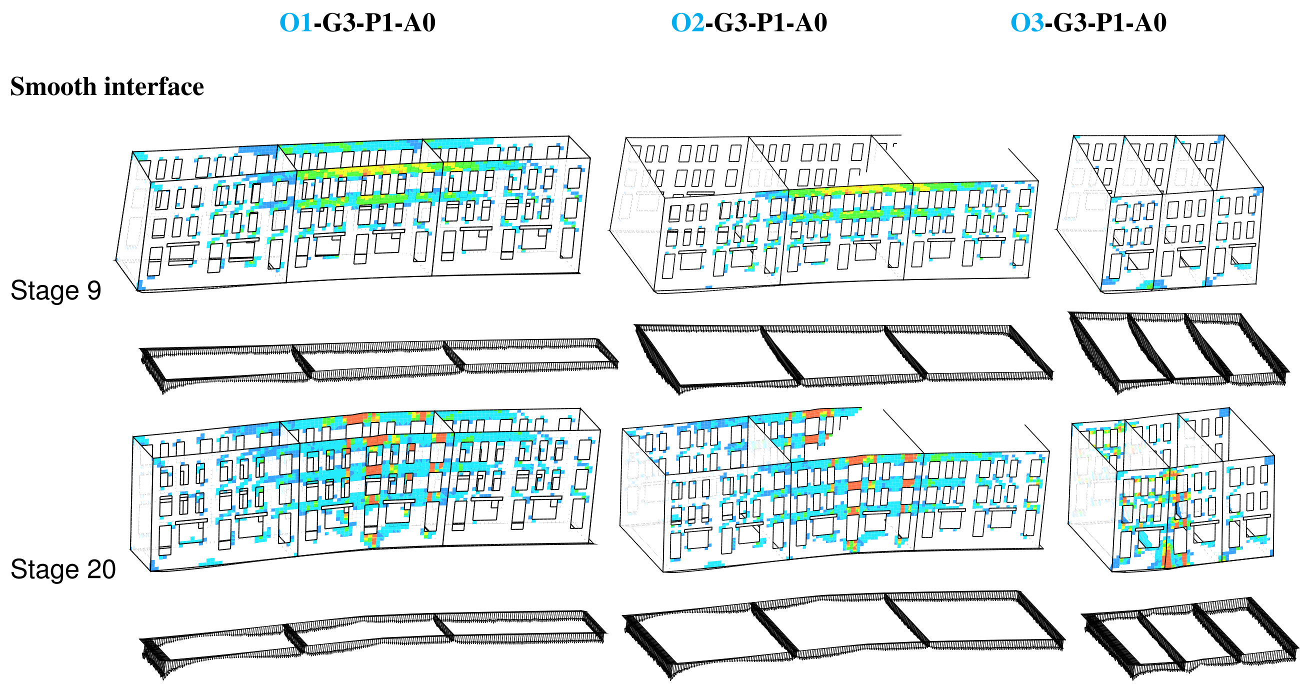

FIG. 6: Crack strain distribution, deformed configuration and soil–structure interface normal stresses: orientation variation for the G3-P1-A0 cases. In Stage 9 the tunnel boring machine passes the building. In stage 20 the machine is fully passed.

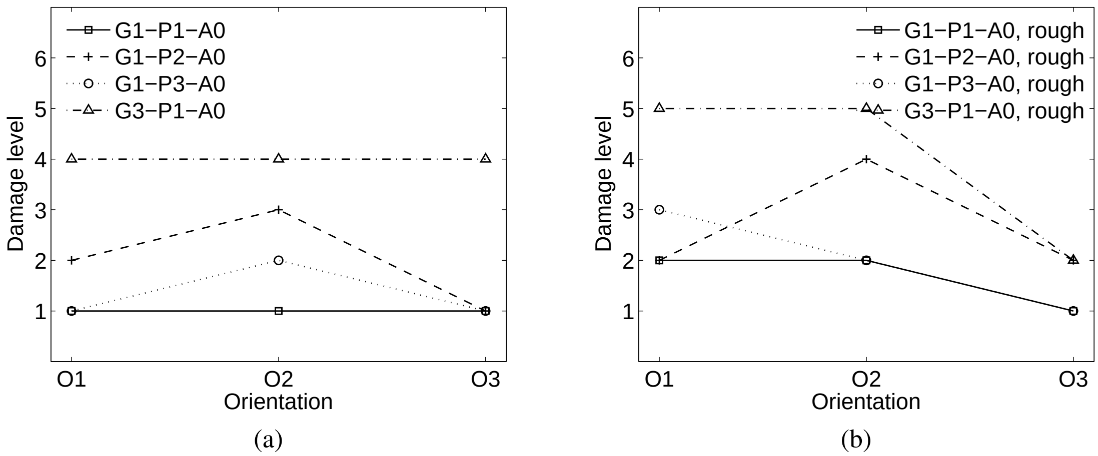

FIG. 7: Damage level as a function of the orientation variations.

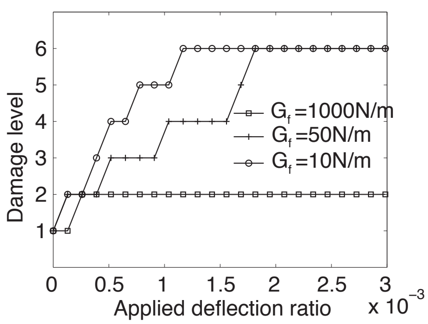

(a) Variation of fracture energy G_f: analyses 4, 3 and reference case

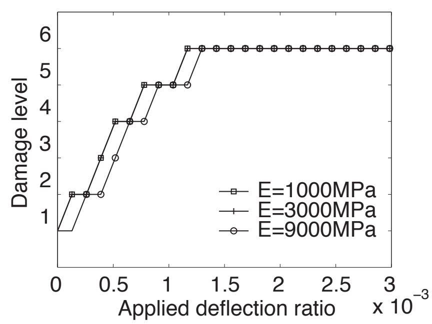

(b) Variation of Young's modulus E: analyses 5, reference case and 6

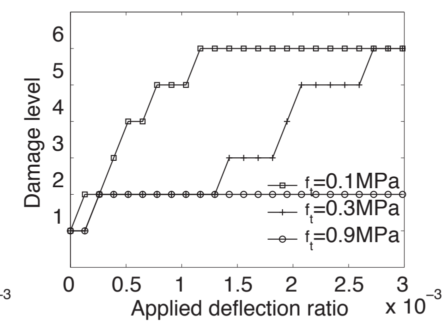

(c) Variation of tensile strength f_t: reference case and analyses 7 and 8

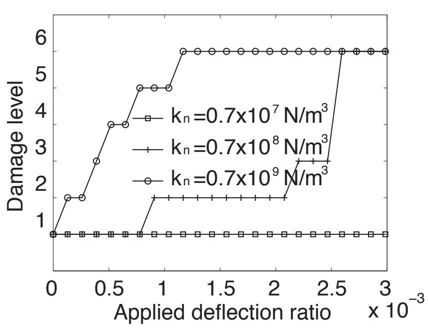

(d) Variation of interface normal stiffness k_t: analyses 9, 10 and reference case

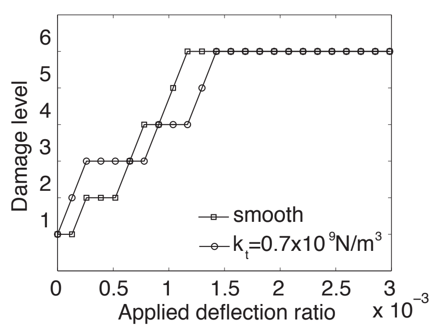

(e) Variation of interface shear behaviour in hogging area: reference case and analysis 11

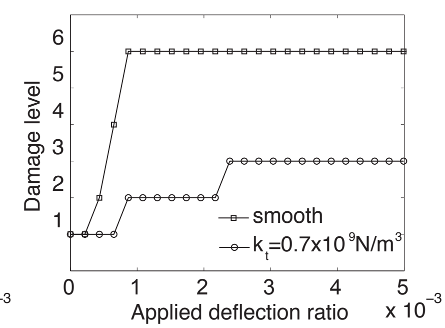

(f) Variation of interface shear behaviour in sagging area: analyses 12 and 13

FIG. 8: Results of the 2D sensitivity study (see Tab. 2).

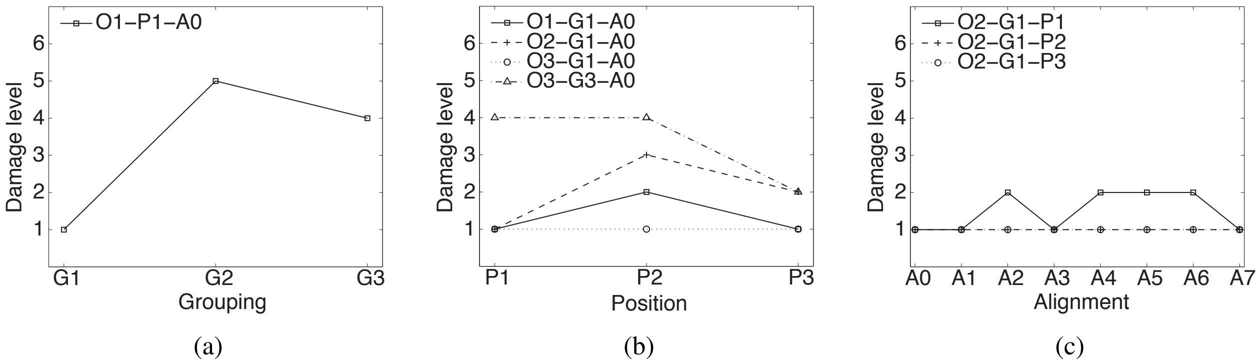

FIG. 9: Results of the 3D sensitivity study (see Tab. 3).

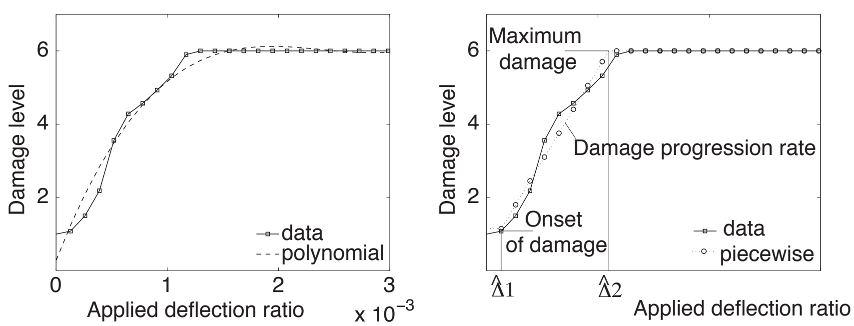

(a) polynomial

(b) piecewise linear

FIG. 10: Numerical curve approximations, 2D reference case.

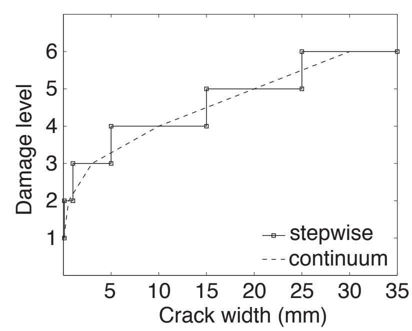

FIG. 11: Maximum crack width vs damage level: step (Tab. 4) and continuous functions.

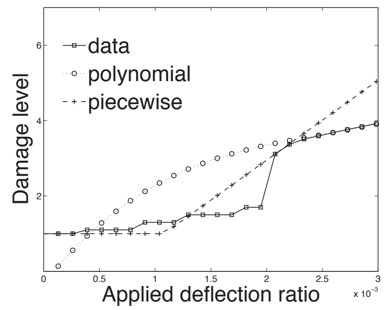

(a1) 0% of openings

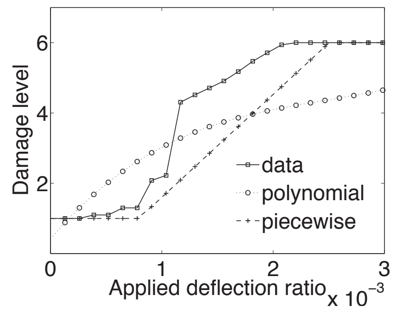

(a2)10% of openings

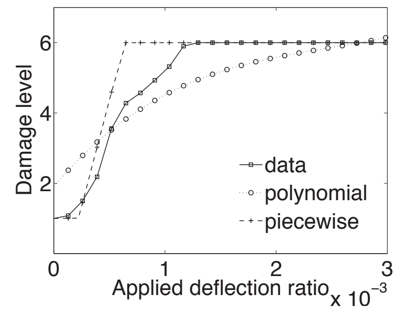

(a3) 30% of openings

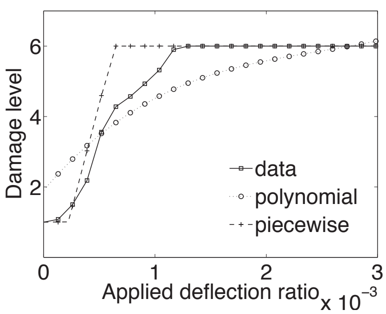

(b1) $G_f = 10$ N/m

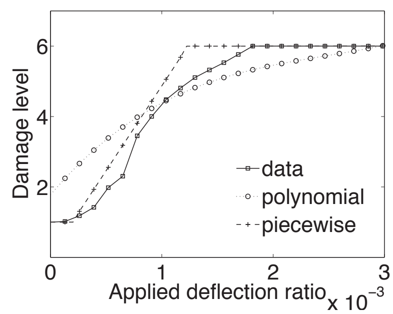

(b2) $G_f = 50$ N/m

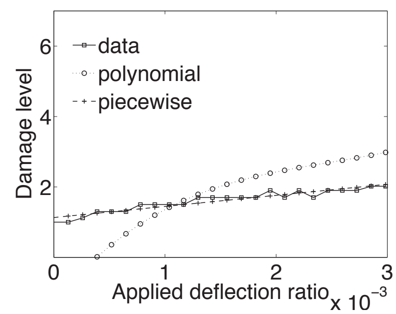

(b3) elastic model

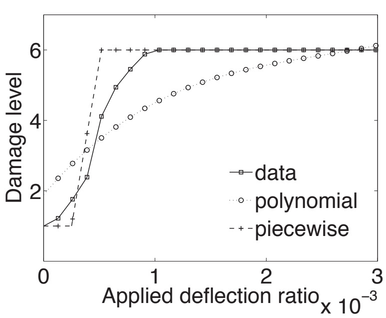

(c1) $E = 1000$ Mpa

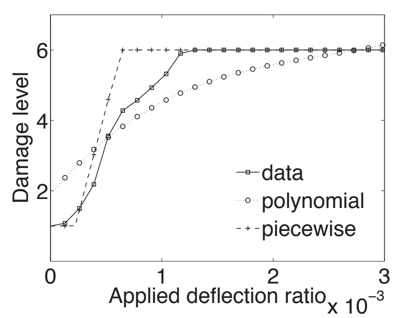

(c2) $E = 3000$ Mpa

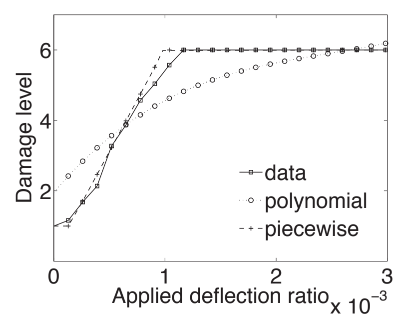

(c3) $E = 9000$ Mpa

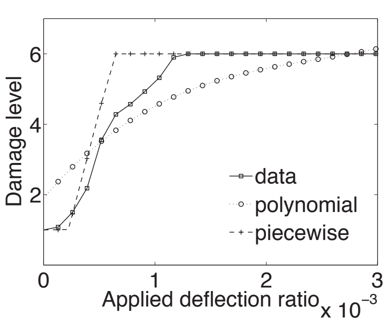

(d1) $f_t = 0.1$ MPa

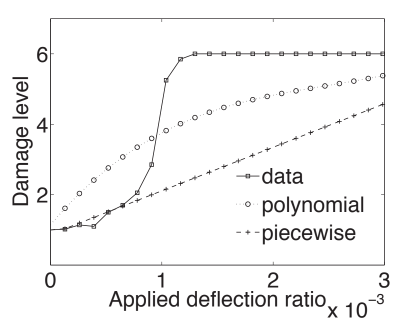

(d2) $f_t = 0.3$ MPa

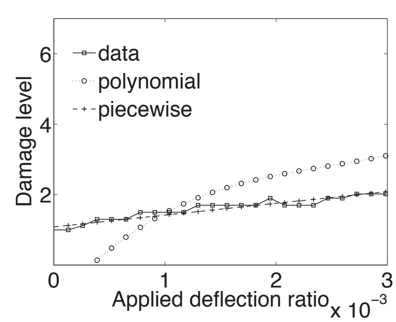

(d3) $f_t = 0.9$ MPa

FIG. 12: Comparison between the observational data and the estimation given by the damage functions.

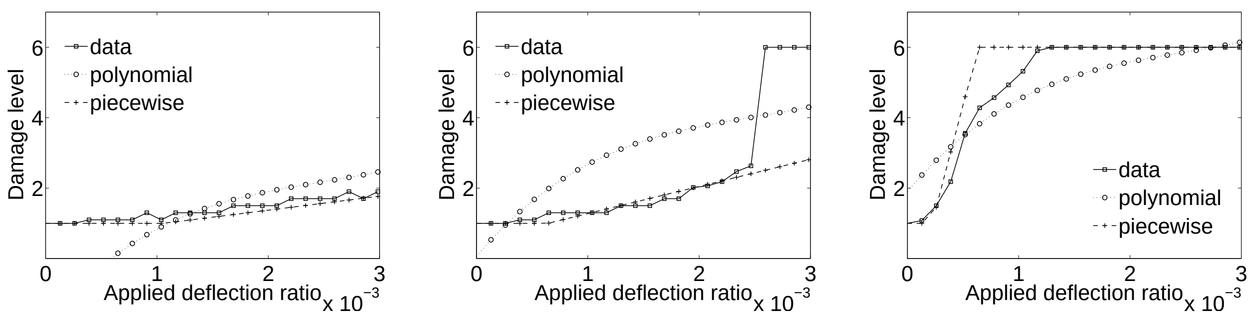

(a1) $k_n = 0.7 \times 10^7 \mathrm{N/m^3}$ (a2) $k_n = 0.7 \times 10^8 \mathrm{N/m^3}$ (a3) $k_n = 0.7 \times 10^9 \mathrm{N/m^3}$

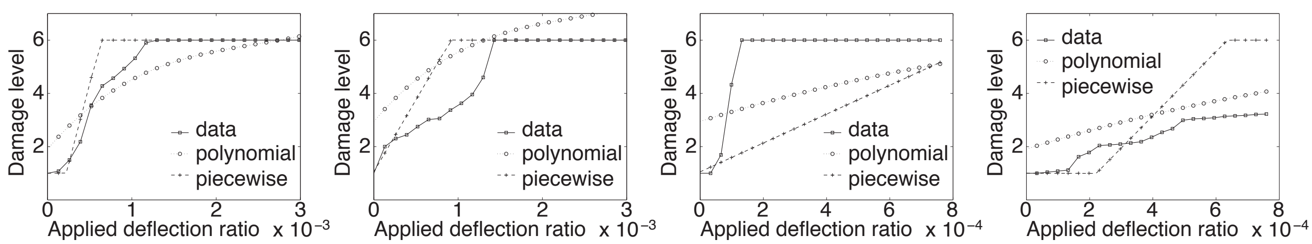

(b1) smooth interface, hogging (b2) rough interface, hogging (c1) smooth interface, sagging (c2) rough interface, sagging

FIG. 13: Comparison between the observational data and the estimation given by the damage functions.

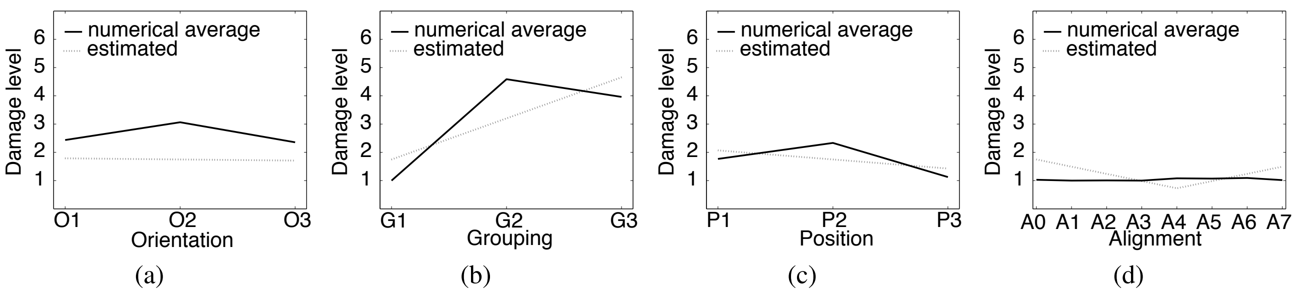

FIG. 14: Comparison between the observational data and the estimation given by the 3D damage function.

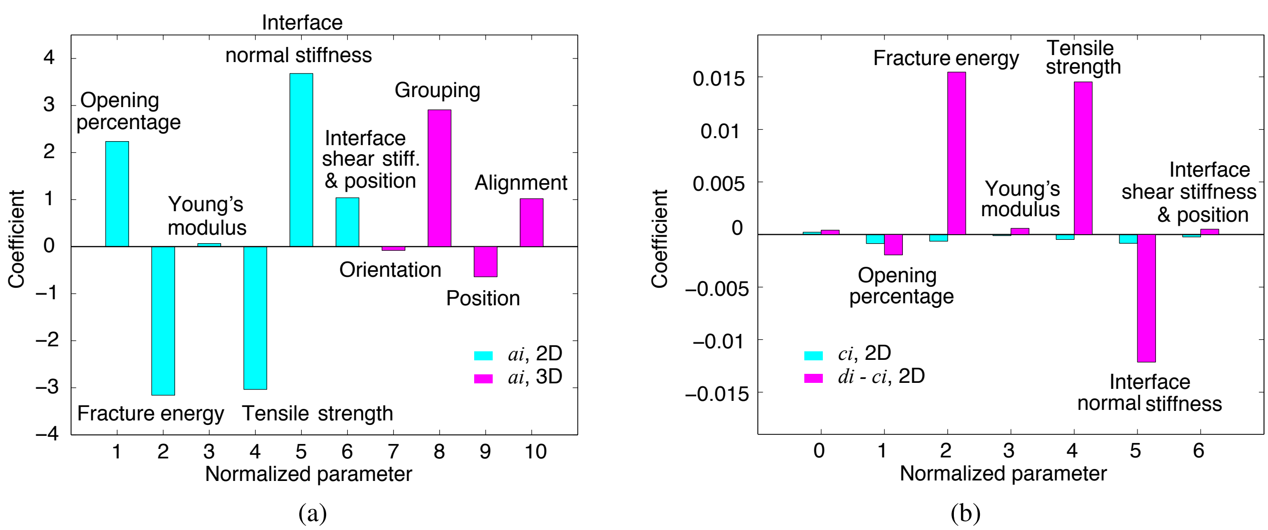

FIG. 15: (a) Coefficients a_i of the polynomial function, as an indication for a possible variation of damage level. The value of each coefficient represents the weight of the corresponding parameter, while the positive or negative sign indicates a positive or negative correlation between the parameter value and the final damage. (b) Coefficients c_i and $d_i - c_i$ of the piecewise function. c_i indicates the effect of each parameter on the deflection ratio at cracking onset, while $d_i - c_i$ measures the parameter influence on the damage increase rate.